

Mössbauer study of ultrathin Fe/Al multilayer films

D. Kaptás,^{1,*} J. Balogh,¹ T. Kemény,¹ L. F. Kiss,¹ L. Bujdosó,¹ A. Kovács,² A. Hirata,² and I. Vincze¹¹Research Institute for Solid State Physics and Optics, 1525 Budapest, P.O. Box 49, Hungary²The Institute of Scientific and Industrial Research, 8-1 Mihogaoka, Ibaraki 567-0047, Osaka, Japan

(Received 20 July 2006; revised manuscript received 10 October 2006; published 11 January 2007)

Multilayers of Fe (between 0.3 and 2.0 nm thickness) separated by a 3.0 nm thick Al spacer were prepared by vacuum evaporation and were then investigated by ⁵⁷Fe Mössbauer spectroscopy measurements between 4.2 and 300 K and in various external magnetic fields. Mixing of the components at the interface was studied by transmission electron microscopy. The formation of a nonmagnetic Al-Fe interface alloy is verified by a detailed analysis of the low temperature Mössbauer spectra. The effective thickness of the Fe layers was deduced from the amount of the nonmagnetic component and it was found to be correlated with the shape of the Fe hyperfine field distribution. A marked change of the temperature and of the external magnetic field dependence of the Fe hyperfine fields were observed as a function of the effective layer thickness. The hyperfine field component attributed to two monolayer thick Fe regions decreases linearly with increasing temperature; it disappears at well below room temperature and it is hardly influenced by external fields up to 7 T. The formation of three and more monolayer thick regions with increasing effective thickness results in an approach to the bulk behavior, $T^{3/2}$ -temperature dependence, and smaller magnetic anisotropy.

DOI: 10.1103/PhysRevB.75.014417

PACS number(s): 75.70.Cn, 75.75.+a, 76.80.+y, 68.35.Fx

I. INTRODUCTION

The study of magnetic multilayers is important both from application (magnetic storage, reading heads, etc.) and fundamental points of view and has been addressed in many review papers.¹⁻⁴ The magnetism of ultrathin layers raises many interesting questions, but in most cases it is difficult to separate the effects of dimensionality from the effects of intermixing between the magnetic and nonmagnetic layers in lack of suitable local investigation methods. There is clear evidence that elements immiscible in equilibrium (e.g., Fe and Ag) will mix to a considerable extent in the boundary region of the thin layers.^{5,6} Unfortunately, in alloys with fcc structure (i.e., in systems consisting of Cu, Ag, Pd, Au, and Pt as nonmagnetic spacer layers) less than 20% of the iron hyperfine field originates from the transfer and conduction electron polarization of the neighboring magnetic moments, the rest is proportional to the Fe atoms' own magnetic moment which is less sensitive to the local neighborhood. On the other hand, in those systems which are amenable to be studied by Mössbauer spectroscopy—since both the Fe magnetic moment and the hyperfine field depends strongly on the Fe nearest neighbor environment (e.g., Fe separated by metalloid spacers)—no epitaxial growth is possible and significant intermixing of the constituents is expected and observed. In the following, we will attempt to separate the effect of intermixing from the thickness dependent magnetic properties.

The Fe-Al system is well suited for such a study as is schematically shown in Fig. 1. Fe is nonmagnetic in the bcc structure with eight nearest neighbors when it has five or more Al first neighbors, $n_{Al} \geq 5$. It has a magnetic moment of about $1.8\mu_B$ with four Al, four Fe nearest neighbors, and $2.2\mu_B$ for $n_{Al} \leq 3$.⁷ Dependence of the Fe hyperfine field on n_{Al} is somewhat more complicated because it is determined by the conduction electron polarization and/or transfer contribution of the nearest and farther magnetic neighbors and

by the polarization of its own core electrons. In the bcc solid solution of α -Fe the latter contribution is proportional to about $6.8 \text{ T}/\mu_B$ to the Fe atoms' own magnetic moment, while the former one will depend on the magnetic moments of the surrounding Fe atoms. As a result,⁸ the nonmagnetic Fe atoms may have hyperfine fields in the neighborhood of magnetic Fe atoms.

Figure 1(b) depicts schematically the three ranges of the expected average values of the Fe hyperfine fields, which overlap to some extent. For nonmagnetic Fe atoms (i.e., $n_{Al} \geq 5$) the source of the hyperfine field is the transfer contribution of the neighboring Fe atoms with magnetic moments, and the distribution of the number and the magnetic moment of these neighbors will contribute to a hyperfine field distribution around a low average value (from 0 to $\approx 12 \text{ T}$). The Fe atoms become magnetic for $n_{Al} = 4$ and the core polarization term appears, thereby causing a sudden increase in the average hyperfine field, but the transfer contribution of the Fe nearest neighbors still depends on the given environment. Since the magnetic moment of the Fe nearest neighbors may vary from 0 to $2.2\mu_B$ the resulting distribution can be rather broad around an average value of ≈ 15 to $\approx 26 \text{ T}$. Finally the Fe atoms with $n_{Al} \leq 3$ will have a distribution of hyperfine fields around even larger average values ($\approx 25 \text{ T}$) due to the increase of both the core and the

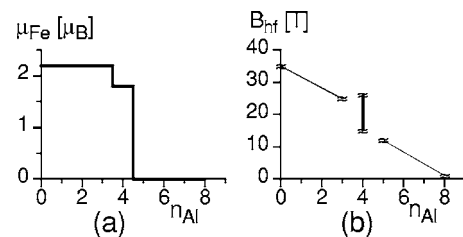


FIG. 1. (a) Dependence of the iron magnetic moment on the number of Al first neighbors and (b) a schematic picture of the three ranges expected for the hyperfine fields as described in the text.

transfer contributions caused by the increased Fe magnetic moments. It is worth emphasizing that the different Fe-Al alloys on the Al-rich side are reported to be nonmagnetic, apart from the incommensurate antiferromagnetic structure of FeAl_2 ,⁸ which is prepared by long-term annealing. However, the hyperfine parameters of this phase are quite different from the values found in the present work.

Most of the earlier investigations of Fe/Al multilayers deal with rather thick (well above 1 nm) Fe layers. The structure of the interface, interdiffusion, and magnetic properties were studied only in a few cases and only room temperature (mostly conversion electron Mössbauer spectroscopy ^{57}Fe measurements⁹⁻¹² were performed. The temperature dependent transmission Mössbauer spectroscopy investigations of the present work represent the first comprehensive study of the development of magnetism in ultrathin layers.

The paper is organized in the following way. Section II describes the details of the sample preparation and the experimental techniques. In Sec. III we present the results that contribute to an understanding of the atomic structure of Fe/Al multilayers. In Sec. III A we determine the ratio of the Fe atoms intermixed with the Al spacers and calculate the resultant correction of the Fe layer thickness. Transmission electron microscopy (TEM) results will be shown to support this evaluation. In Sec. III B it will be shown that the calculated effective Fe layer thickness and the hyperfine parameters of the layers are in line. Section IV deals with the magnetic properties. Section IV A presents the temperature dependence of the Fe hyperfine fields as a function of the Fe layer thickness where a crossover from linear to $T^{3/2}$ behavior is observed. The measurements in various external magnetic fields are presented in Sec. IV B: The observed strong magnetic anisotropy will also be shown to correlate with the deduced effective Fe layer thickness. Finally, in Sec. V a summary of the results is presented.

II. EXPERIMENT

The samples were evaporated onto Si(111) wafers in a vacuum of 10^{-7} Pa with an evaporation rate of approximately 0.1 nm/s. The substrate was first coated by 10 nm Ag before the evaporation of the first Al layer to ensure that the samples could be removed from the substrate. The topmost layer was 200 nm Al to protect the multilayer from oxidation. Ag and Al were evaporated by two electron guns, the Fe (^{57}Fe) was evaporated from a heated W crucible. The layer thickness was controlled by a quartz oscillator and the nominal layer thickness, t_{nom} , is given using bulk density data. The thickness of the Al layers was kept at $t_{\text{Al}}=3.0$ nm, and while the thickness of the Fe layers in the ^{57}Fe enriched samples was increased from $t_{\text{nom}}=0.3$ to 1.0 nm, the number of Fe layers was decreased from 15 to 6. This series was supplemented with a sample of $t_{\text{nom}}=2.0$ nm prepared from natural Fe; in this case, the number of Fe layers was 32. The measurements were performed on a single film removed from the Si substrate, then cut into pieces and stacked to give the appropriate thickness for Mössbauer measurements.

^{57}Fe Mössbauer spectra between 4.2 and 300 K, with and without external magnetic fields were recorded by a standard

constant acceleration spectrometer using a 50 mCi $^{57}\text{CoRh}$ source at room temperature. The magnetic field was applied parallel to the γ -beam using a 7 T Janis superconducting magnet. Mössbauer measurements as a function of temperature were also performed in a closed cycle refrigerator. The spectra were evaluated in a standard manner; binomial distributions¹³ were used to describe the distributions of the hyperfine parameters. Isomer shift data are given with respect to α -Fe at the given temperatures.

The cross sectional samples for the TEM analysis were attained in the conventional manner, that is, face-to-face gluing, cutting of thin slices, mechanically polishing and, finally, ion-milling. The preparation was completed by low energy ion milling at 200 eV to remove the surface damaged and amorphized layer. Structure analysis was carried out by a LEO-922 TEM equipped with a Ω -type energy filter operated at 200 kV. The three-window technique was applied to get the net element-selective image.

III. THICKNESS DEPENDENCE OF THE IRON LAYER FORMATION

A. Interface mixing

The ^{57}Fe Mössbauer spectra measured at 4.2 K and at room temperature are shown in Fig. 2. The quadrupole dou-

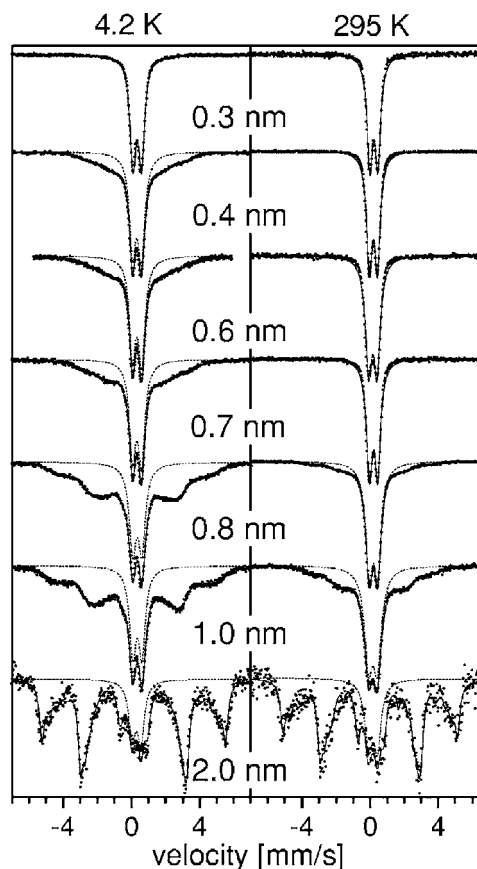


FIG. 2. Mössbauer spectra of Fe/Al multilayers measured at 4.2 K and at room temperature as a function of the nominal Fe thickness, t_{nom} . The paramagnetic quadrupole doublet corresponding to Fe atoms alloyed or intermixed with Al layers is shown by a dotted line.

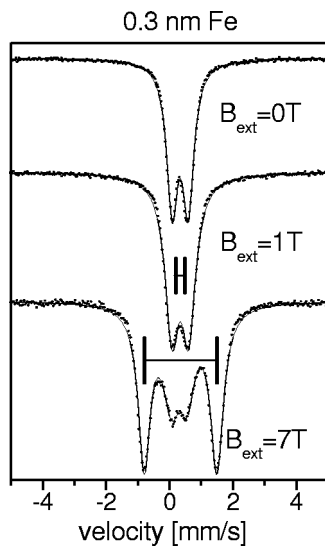


FIG. 3. Mössbauer spectra of the Fe(0.3 nm)/Al(3 nm) multilayer at 4.2 K in different applied fields. The bars indicate the splitting equivalent to the applied field.

blet observed at 4.2 K in all the spectra should belong to nonmagnetic Fe atoms surrounded by Al atoms, therefore it is attributed to Fe atoms alloyed with the Al layers. For $t_{\text{nom}}=0.3$ nm only the quadrupole doublet component is present; all the Fe atoms intermix with the Al spacer layers. This doublet clearly corresponds to nonmagnetic Fe atoms, the presence of superparamagnetic clusters was ruled out by measurements in a magnetic field. As is shown in Fig. 3, only the magnetic splitting due to the applied external magnetic field can be observed up to 7 T at 4.2 K.

The parameters of the quadrupole doublet subcomponent agree well for all the spectra shown in Fig. 2, i.e., it does not depend on the Fe layer thickness. These nonmagnetic Fe atoms are clearly not in the vicinity of magnetic Fe layers or particles; otherwise, they would have a hyperfine field due to the transfer contribution of the nearby magnetic moments. Since the magnetic splitting disappears below 295 K between $t_{\text{nom}}=0.4$ and 0.7 nm and the different paramagnetic components strongly overlap, accurate determination of the room temperature parameters is possible only in the case of the $t_{\text{nom}}=0.3$ nm sample. The Mössbauer spectrum of the nonmagnetic Fe atoms consists of a slightly broadened quadrupole doublet with the room temperature parameters: 0.22 mm/s, 0.47 mm/s, 0.39 mm/s for the isomer shift (IS), quadrupole splitting (ΔE_Q), and linewidth (2Γ), respectively. At low temperatures only a slight increase of the quadrupole splitting (to 0.50 mm/s at 4.2 K) is observed. The quadrupole splitting and the isomer shift observed for the nonmagnetic Fe atoms agree with those of Al_5Fe_2 , as was found in earlier studies.^{9–12,14–18}

The interface structure was studied by energy filtered TEM in the case of the 0.3 and 0.4 nm nominal Fe thickness samples where, according to the Mössbauer results of Fig. 2, the magnetic phase is not present at all or only to a rather limited extent. Since very similar results were obtained for the two samples, images will be shown only for the second sample. The bright field and the energy filtered images are

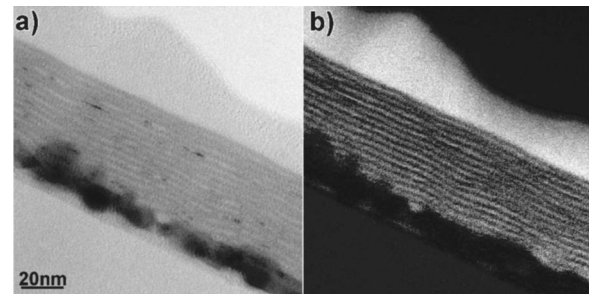


FIG. 4. Energy filtered TEM analysis of the Ag(10 nm)/Al(5 nm)/[Al(3 nm)/Fe(0.4 nm)]₁₅/Al(200 nm) multilayer sample. (a) Bright field image and (b) corresponding energy-filtered image indicating the distribution of Al.

presented in Fig. 4. The sample structure starts with an Ag layer giving dark contrast on the bright field image [Fig. 4(a)] and it is followed by the multilayer structure of Al and Fe with periodic light and dark contrasts. The Al-cap layer is visible on the top of the sample. The Al-elemental mapping by appropriate energy filtering [Fig. 4(b)] also shows the light and dark layer periodicity, which coincides with the layers on the bright field image. The electron diffraction and high-resolution analyses (not shown here) revealed the presence of crystalline Al and a disordered amorphouslike Al-Fe phase. These findings agree well with those of Ref. 15. On the basis of these results, the light-contrast layers belong to the pure Al phase and the dark-contrast areas contain Fe. The composition of the Fe containing layers can only be estimated from the average width of the pure Al layers. On average, the light and the dark contrast layers seem to be equal in width, which supports the concept that the alloyed regions have a composition close to that of Al_5Fe_2 , as deduced from the Mössbauer parameters. Bearing in mind the small thickness (≈ 1.8 nm) and the disordered nature of the interface zone one should think rather of local coordinations similar to that in Al_5Fe_2 than of long range periodicity. Details of the solid state reaction that takes place during the deposition of the Fe and Al layers are not well understood^{9–12,14,15,19–23} and the formation of nonequilibrium phases (amorphous or nanostructured) cannot be ruled out.

In the Mössbauer analysis the area under the nonmagnetic doublet is proportional to the amount of those Fe atoms mixed with the Al spacer. The relative fraction, f_p , is shown in Fig. 5 as a function of t_{nom} . Here $t_D=f_p t_{\text{nom}}$ is the total number of Fe atoms (as given in equivalent Fe thickness) mixed with the Al spacer. This t_D is roughly constant for the whole investigated t_{nom} range with the value of $t_D \approx 0.31$ nm. The formation of a continuous layer of the Al_5Fe_2 -like interface alloy can explain this result. It means that t_{nom} should be decreased by t_D to obtain the effective Fe layer thickness, $t_{\text{eff}}=t_{\text{nom}}-t_D$. The formation of a magnetic Fe layer was not observed for $t_{\text{nom}}<0.4$ nm, a factor that supports this picture. It is also plausible that the magnetic component with $t_{\text{eff}}=0.1$ nm cannot be separated in the TEM images of Fig. 4. Preliminary results indicate traces of crystalline Fe for $t_{\text{eff}}=0.5$ nm.

B. Thickness dependence of the hyperfine field distribution

After analyzing the variation of the ratio of the paramagnetic component, we will discuss the thickness dependence

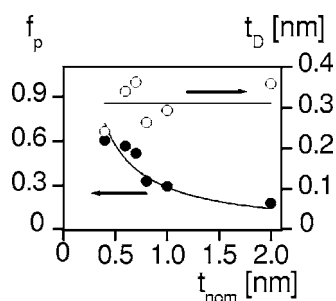


FIG. 5. The fraction of the paramagnetic quadrupole doublet f_p (dots) and $t_D = f_p t_{\text{nom}}$ (circles) as a function of the nominal thickness t_{nom} of the Fe layers. The lines are to guide the eye.

of the magnetic component in order to gain insight into the atomic structure of the magnetic layers. The hyperfine distributions calculated by allowing two binomial distributions¹³ are shown in Fig. 6. The distributions clearly show a bimodal character above $t_{\text{nom}} = 0.7$ nm.

It is known²⁴ from investigations into the ordered $B2$ structure FeAl alloy that a single Fe layer between Al sheets is nonmagnetic. In this case, the Mössbauer spectrum consists of a single nonmagnetic line due to the cubic environment. Such a component was not revealed in any of the spectra but, because of the strong overlap of the different

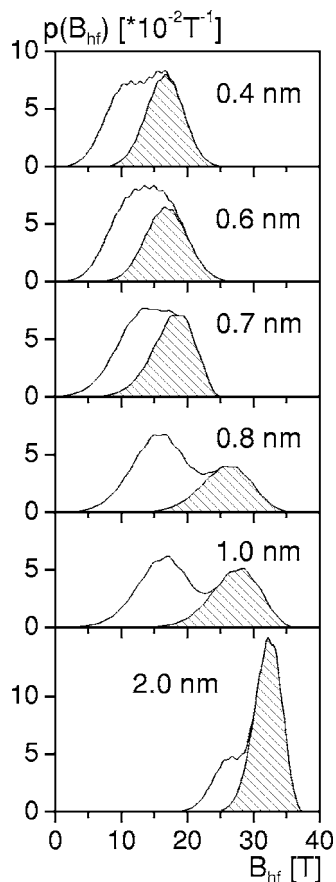


FIG. 6. Distribution of the Fe hyperfine field of the magnetically split component of the Mössbauer spectra at 4.2 K as a function of t_{nom} . The lightly shaded area marks the high field component (see text for details).

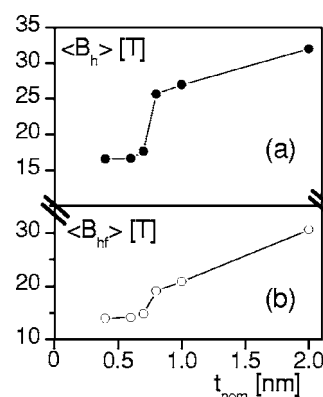


FIG. 7. Average hyperfine field of the high field component of the hyperfine field distribution $\langle B_h \rangle$ (a) and (b) the average hyperfine field of the full distribution $\langle B_{\text{hf}} \rangle$ at 4.2 K are shown as a function of t_{nom} .

components around zero velocity, a small contribution of this kind cannot be excluded.

In two monolayer (ML) thick Fe planes between Al layers all the Fe atoms have four Fe and four Al nearest neighbors, and these layers would be magnetic according to Fig. 1. In cold-worked Fe-Al alloys with $B2$ structure the appearance of ferromagnetism around 35–40 at. % Al content was indeed attributed to two or more Fe atom thick layers formed around antiphase grain boundaries.²⁵ In ball-milled stoichiometric bcc FeAl alloys the grain boundaries were also identified as two atom thick Fe layers based on the evidence of x-ray diffraction and Fe hyperfine field distribution measurements.²⁶ In this case the Fe hyperfine fields were terminated below ≈ 25 T, which is a clear indication of the absence of Fe atoms with more than four Fe first neighbors [see Fig. 1(b)]. In the present case the Fe hyperfine field distributions, $p(B)$ deduced from the magnetically split part of the spectra, as shown in Fig. 6, are rather similar between $t_{\text{nom}} = 0.4$ and 0.7 nm to those of Ref. 26. The isomer shift of these magnetically split spectra is 0.20(1) mm/s (with respect to α -Fe at 4.2 K), in good agreement with the value for Fe atoms with four Fe, four Al nearest neighbors in the Fe_3Al structure [0.19(1) mm/s].²⁷ These are strong indications that only Fe layers consisting of two atomic planes are formed in this thickness range, which is in line with the t_{eff} values for these samples. Obviously, the mixing of Al into the two monolayer thick Fe layers will result in nonmagnetic Fe atoms and thus in the interruption of the continuous magnetic structure. In view of this, the two atom thick Fe layers are platelet shaped particles with a broad lateral size distribution rather than continuous periodic layers, but the extent of the platelets is expected to increase with increasing t_{nom} .

A significant change is observed at $t_{\text{nom}} = 0.8$ nm: A high field component appears in the Mössbauer spectrum and of course, in the calculated hyperfine field distribution. This indicates that the two monolayer (ML) effective Fe layer thickness is exceeded and the building up of a third layer starts. Fe atoms in the middle Fe layer of a perfect three-layer structure have eight Fe first neighbors and thus significantly higher hyperfine fields. Figure 7 shows the average hyperfine field of the high field part of the distribution, $\langle B_h \rangle$ together

with the average hyperfine field of the full hyperfine field distribution, $\langle B_{\text{hf}} \rangle$. (The values of $\langle B_{\text{hf}} \rangle$ are burdened with larger systematic errors than $\langle B_h \rangle$ due to the nonmagnetic component in the middle of the spectra, thus most of our discussion in the following will be based on the analysis of the outer lines of the spectra, i.e., on $\langle B_h \rangle$. Note the large jump in both values between $t_{\text{nom}}=0.7$ and 0.8 nm which signals the formation of Fe layers consisting of at least three atomic planes. If the Fe layer were to consist of exactly three atomic planes, the ratio of the areas under the high and the low field part of the distribution should be 1:2, which is quite close to the ratio observed for the $t_{\text{nom}}=0.8$ nm sample. This is in line with the $t_{\text{eff}}=0.5$ nm value calculated for this sample. The agreement between the number of atomic planes in the Fe layers deduced from the shape of the hyperfine distribution and the effective Fe layer thickness is reassuringly good. It is very tempting to explain our result on the development of three ML thick Fe layers for $t_{\text{eff}}=0.5$ nm by the formation of a DO_3 type local Fe_3Al alloy which would give the same 1:2 ratio of the high-field/low-field components. However, the values of the hyperfine fields are quite different: In our case at 4.2 K they are 25.7 and 15.0 T compared to the extrapolated values²⁸ of 32.6 and 23.4 T in Fe_3Al . Disorder and Al surplus in the Fe_3Al structure could explain the lower hyperfine field values but it would cause a significant deviation in the site occupancies.

As t_{nom} is increased further $\langle B_h \rangle$ and $\langle B_{\text{hf}} \rangle$ keep increasing as shown in Fig. 7; however, the value of the hyperfine field of pure α -Fe (33.8 T) is not reached even at $t_{\text{nom}}=2.0$ nm. For a perfect layer structure the appearance of a sharp six-line pattern with 33.8 T hyperfine field is expected, which would correspond to the inner Fe layers. Its absence and the presence of low field satellite components in the spectra of Fig. 2 are clear indications of Al dissolved in the iron layers. The increase of $\langle B_h \rangle$ and $\langle B_{\text{hf}} \rangle$ with increasing Fe layer thickness is explainable by the increasing average Fe magnetic moment which results in an increase of both the nonlocalized contribution of the further Fe neighbors (conduction electron polarization) and the localized contribution of the nearest Fe neighbors to the hyperfine field.

Although Al has large equilibrium solubility in α -Fe (about 20 at. %), a substantially lesser amount is dissolved in the Fe layers. For our thickest sample, $t_{\text{nom}}=2.0$ nm ($t_{\text{eff}}=1.7$ nm), the hyperfine field distribution has a structure quite different from that expected for a pure layer. This structure originates both from Al dissolved in the Fe layers and from interface effects. The Fe atoms near the edge of the layer—not only those at the edge—will have a smaller transfer contribution and thus reduced hyperfine field values. Assuming complete random distribution of the Al atoms in the layer and neglecting the interface effect the amount of dissolved Al, c_{Al} may be estimated from the ratio under the areas of the largest hyperfine field sextet to the next largest hyperfine field sextet as $8c_{\text{Al}}/(1-c_{\text{Al}})$, whose ratio in dilute alloys gives²⁹ the relative number of Fe atoms with a single Al first neighbor. This oversimplified estimation gives about 6 at. % Al dissolved in the Fe layers.

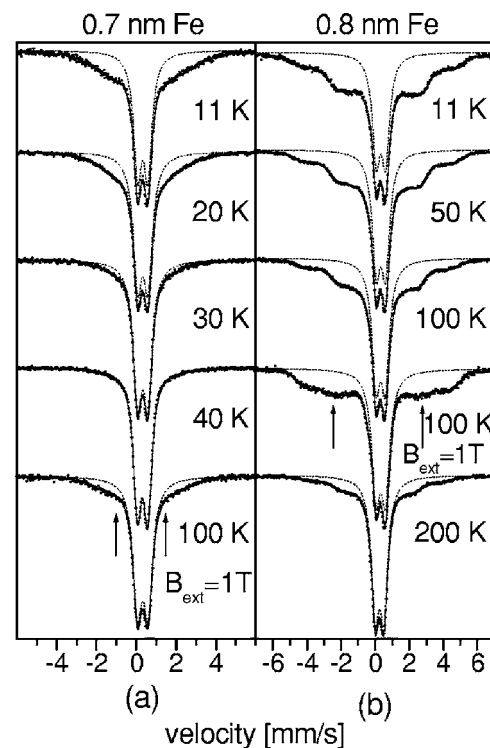


FIG. 8. Temperature dependence of the Mössbauer spectra of the (a) Fe(0.7 nm)/Al(3 nm) and (b) Fe(0.8 nm)/Al(3 nm) samples in zero external magnetic field and in $B_{\text{ext}}=1$ T at 100 K. For the latter, the positions of the 2–5 lines of the B_h components of the spectra are marked by arrows.

IV. MAGNETIC PROPERTIES

A. Temperature dependence of the hyperfine fields

The temperature dependence of the magnetization, the nature of the magnetic phase transition, and the role of the magnetic anisotropy in ultrathin films belong to the most often investigated fundamental problems.^{1–4,30–33} Even so, the results obtained are still controversial.

The temperature dependence of the magnetization of our samples will be studied by evaluating $\sigma(T) = \langle B_h(T) \rangle / \langle B_h(4.2 \text{ K}) \rangle$, since the high field components of the hyperfine distribution are influenced the least by the paramagnetic components of the spectra and in this way the systematic errors are minimized. A different type of behavior is observed for $t_{\text{nom}} \leq 0.7$ nm and for $t_{\text{nom}} \geq 0.8$ nm, i.e., for samples containing platelets of two ML Fe planes and for those with three or more monolayers. Typical Mössbauer spectra are shown in Fig. 8.

Layers with three or more Fe atomic planes show well-defined magnetic splitting even at room temperature indicating a rather high Curie point. The $\sigma(T)$ curves follow well the Bloch law, $\sigma(T) = 1 - b_i T^{3/2}$ as shown in Fig. 9(a). (A fit with T^2 temperature dependence is significantly worse. We would also mention that at low temperatures no upturn of the magnetization³⁴ was observed.) The respective spin wave parameter, b_i values are $b_i = 42.2, 53.3,$ and $10.3 \times 10^{-6} \text{ K}^{-3/2}$ for $t_{\text{nom}} = 0.8, 1.0,$ and 2.0 nm, i.e., for $t_{\text{eff}} = 0.5, 0.7,$ and 1.7 nm, while the bulk value of the spin wave parameter is

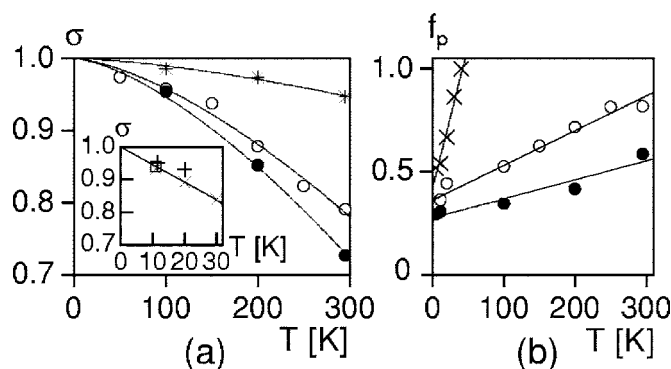


FIG. 9. (a) $\sigma = \langle B_h(T) \rangle / \langle B_h(4.2 \text{ K}) \rangle$ as a function of temperature for $t_{\text{nom}} = 2.0$ nm (*), 1.0 nm (●), and 0.8 nm (○), respectively. The continuous lines correspond to a $T^{3/2}$ dependence. The inset shows σ for $t_{\text{nom}} = 0.7$ nm (×), 0.6 nm (+), and 0.4 nm (□). The continuous line is the linear fit for $t_{\text{nom}} = 0.7$ nm. (b) Temperature dependence of the fraction of the paramagnetic quadrupole doublet f_p for $t_{\text{nom}} = 0.7$ nm (×), 0.8 nm (○), and 1.0 nm (●). The lines are to guide the eye.

$b_\infty = 5.2 \times 10^{-6} \text{ K}^{-3/2}$. In ultrathin Fe films on different substrates b_t/b_∞ was found³⁵ to increase linearly with the inverse thickness of the layer. Our data follow roughly the trend established³⁵ by the Fe(001)/Au(001) and Fe(001)/GaAs(001) epitaxial ultrathin Fe films. The increase of b_t when the Fe thickness increases from $t_{\text{nom}} = 0.8$ to 1.0 nm is most probably caused by differences in the shape of the magnetization curves, as is the case^{28,29} for α -Fe and Fe₃Al.

The f_p value increases with increasing temperature as shown in Fig. 9(b) — except for $t_{\text{nom}} = 2.0$ nm — where no detectable increase was found. A similar increase was observed above room temperature in Ref. 9. It is a fingerprint of superparamagnetic particles present in the samples. In the analysis of magnetization measurements this is a serious obstacle, but in our Mössbauer experiments the paramagnetic contribution can be separated and does not influence the results obtained for the magnetic component, especially since they are deduced from the high field part of the hyperfine field distributions.

It is hard to estimate the Curie temperatures, T_C , of our samples since the measurements could be performed only in a limited temperature range. The value of σ at room temperature is 0.976 in α -Fe²⁹ ($T_C = 1041$ K) and 0.90 in Fe₃Al²⁸ ($T_C = 710$ K, but values up to 770 K are reported depending on the degree of the DO₃-type order). Thus Fig. 9(a) indicates a T_C lower than that of Fe₃Al for $t_{\text{nom}} = 0.8$ and 1.0 nm, and a T_C higher than that for the 2.0 nm thick sample. The actual values should be determined from the shape of the $\sigma(T/T_C)$ curves. These are, however, significantly different^{28,29} for α -Fe and Fe₃Al: σ of the latter is smaller for the same T/T_C value. The extrapolated T_C values are 390, 360, and 720 K if the $\sigma(T/T_C)$ curve of α -Fe, and 520, 450, and 1180 K if that of Fe₃Al is used for $t_{\text{nom}} = 0.8$, 1.0, and 2.0 nm, respectively. The latter set is obviously an overestimation; the former set is probably an underestimation of the T_C values. Curie temperatures of Fe/Al multilayered films were determined³⁶ from magnetization versus temperature

curves measured in a 1 kG field for Fe layer thicknesses from 0.5 to 20 nm and all the T_C values were between 430 and 630 K. However, the deduced T_C is ambiguous because application of the magnetic field caused significant changes of the magnetization curves and T_C was considerably less than that of pure iron even for the thickest sample, which hints at a significant intermixing due to the high measuring temperatures.

Substantially different behavior is found for $t_{\text{nom}} \leq 0.7$ nm: The magnetically split part of the spectra disappears well below room temperature and $\sigma(T)$ decreases linearly with temperature. These features can be associated with the superparamagnetic relaxation of small particles. Magnetic splitting cannot be observed in the spectra above $T_f = 15, 25$, and 40 K for $t_{\text{nom}} = 0.4, 0.6$, and 0.7 nm, respectively. This characteristic temperature is termed as freezing temperature, T_f , to distinguish it from the usual blocking temperature, T_B , being commonly defined by an equal fraction of the ferromagnetic and paramagnetic spectrum components.

The observed linear temperature dependence of the hyperfine field is expected^{37,38} for superparamagnetic particles. The assumption of a uniaxial anisotropy with anisotropy constant K_{eff} for the particles with volumes V is the simplest approximation which results in

$$\sigma(T) = 1 - CT, \quad (1)$$

where $C = k_B / 2VK_{\text{eff}}$ and k_B is Boltzmann's constant. This approach should be applied³⁷ only for temperatures $k_B T / VK_{\text{eff}} \approx 0.1 - 0.2 \ll 1$. We found $C = 5.4 \times 10^{-3} \text{ K}^{-1}$ for the 0.7 nm Fe/3.0 nm Al sample [Fig. 9(a)]. Linear temperature dependence of the magnetization and/or hyperfine field was found^{2,3,37} in ultrathin, 2–3 ML thick films. Our calculated C value is larger than that found³⁷ in two ML thick Fe on Ag [$(1.5 - 5.7) \times 10^{-4} \text{ K}^{-1}$] or that of three ML thick Fe on Pt ($3 \times 10^{-3} \text{ K}^{-1}$).³

Superparamagnetic behavior is also indicated by the reappearance of the magnetic splitting above the freezing temperature when a magnetic field is applied, as shown in Fig. 8 for $B_{\text{ext}} = 1$ T. This feature can be used to estimate the size of the magnetic particles, since the high-field expansion of the Langevin function gives^{39,40}

$$\langle B_h(T) \rangle + B_{\text{ext}} = B_0(1 - C_B T), \quad (2)$$

where B_0 is the saturation hyperfine field, $C_B = k_B / \mu B_{\text{ext}}$, and μ is the magnetic moment of the particle. $C_B = 1.4 \times 10^{-3} \text{ K}^{-1}$ was obtained at $T = 100$ K, $B_{\text{ext}} = 1$ T for the 0.7 nm Fe/3.0 nm Al sample. It gives $\mu \approx 1000 \mu_B$, which in turn corresponds to about 570 Fe atoms in the particle, when the extrapolated value of $1.8 \mu_B$ of the magnetic moment of the Fe atoms with 4 Fe, 4 Al nearest neighbors is used. The particle volume is $V \approx 6.8 \text{ nm}^3$, and a spherical shape of these particles would correspond to a diameter of 2.4 nm. Combination of this value of the particle volume with the value of C allows the determination of the effective magnetic anisotropy constant, which gives $K_{\text{eff}} = 1.9 \times 10^5 \text{ J/m}^3$. This value is significantly larger than the volume anisotropy constant for α -Fe ($\approx 0.5 \times 10^5 \text{ J/m}^3$). It is about the same value obtained³⁹ for nanoparticles of metallic iron with similar size

where the increase is attributed to the influence of surface anisotropy. The combined treatment⁴¹ of the effect of magnetic anisotropy and applied field would result in about 20% smaller particle volume and consequently in larger magnetic anisotropy constant.

It has already been discussed that the hyperfine field distribution of these thin layers excludes the presence of 3 ML thick regions, thus the assumption of a squared brick shape is more appropriate. If the lateral size of these bricks is L , then $V=2aL^2$, where $a=0.15$ nm is the distance between the Fe planes. This approximation gives a characteristic size of $L=4.7$ nm.

A rough estimation of the island size is also possible by taking into account the effect of Al atoms dissolved in the Fe layers. A single Al atom dissolved in a perfect two Fe atom thick layer will result in four nonmagnetic Fe atoms. These nonmagnetic Fe atoms together with the Al atoms will isolate the magnetic islands. The relative amount of Al dissolved in the Fe layer is $c_{\text{Al}}/c_{\text{Fe}}=4La^2/2aL^2=2a/L$ if the boundary of the Fe islands consists of Al atoms alone. This is obviously an oversimplification of the real Al percolation problem which gives an estimation of the characteristic island size, as $L=2a(1/c_{\text{Al}}-1)$. The formerly estimated $c_{\text{Al}}\approx 6$ at. % value of the amount of Al dissolved in the Fe layer also results in $L=4.7$ nm. These magnetic islands are at only a few atomic distances from each other; therefore, a strong interaction is expected between them and the validity of Eqs. (1) and (2) may be questioned.

B. Effect of external magnetic field

The relative intensity of the 2–5 lines with respect to the 3–4 lines of a six-line Mössbauer spectrum is given as $I_{2-5}=4\sin^2\theta/(1+\cos^2\theta)$, where θ is the angle between the direction of the γ rays and the magnetization of the sample. $I_{2-5}=4$ corresponds to the case when all the magnetic moments are in the plane of the sample. In general $I_{2-5}=2$ signals the completely random distribution of the direction of the magnetic moments, except for the case of a special magnetic anisotropy, when $\cos^2\theta=1/2$ gives the same I_{2-5} value. In an external magnetic field applied parallel to the direction of the γ rays the full magnetic saturation is characterized by the value $I_{2-5}=0$, i.e., the 2–5 lines of the spectra disappear.

The absolute value of the hyperfine field also contains information on the orientation of the magnetic moments. The hyperfine field is oriented antiparallel to the magnetic moment; thus in collinear ferromagnets the absolute value of the measured hyperfine field will decrease with the value of the applied field and increase with the value of the demagnetizing field of the sample. If the magnetic moments are not collinear with the applied field, the decrease is only $B_{\text{ext}}\cos\theta$. The hyperfine field of antiferromagnetically coupled magnetic moments will increase with the applied field.

The measurements performed in applied magnetic fields are consequently suitable as a means to study the orientation of the magnetic moments, the approach to magnetic saturation, and to gain information on the magnetic anisotropy. The Mössbauer spectra measured in different external magnetic

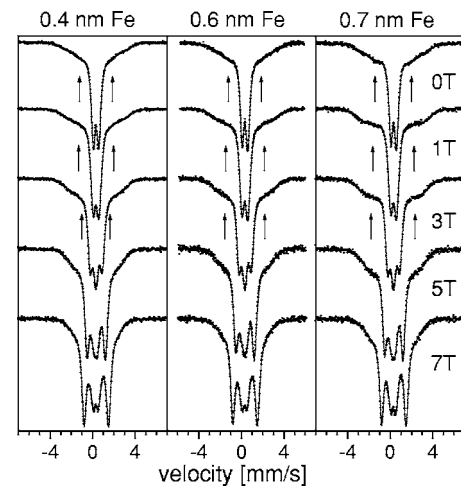


FIG. 10. Mössbauer spectra at 4.2 K in external magnetic fields B_{ext} applied perpendicularly to the sample plane of the $t_{\text{nom}}=0.4$, 0.6, and 0.7 nm samples. The positions of the 2–5 lines belonging to $\langle B_h \rangle$ are marked by arrows for $B_{\text{ext}}=0$, 1, and 3 T, respectively.

fields are shown in Figs. 10–12. They show two features common to all the spectra. First, no increase of the hyperfine fields of the magnetic component, i.e., no evidence for the existence of antiferromagnetically oriented magnetic moments can be found. Second, the applied field induces the appearance of magnetic splitting in the case of the nonmagnetic Fe atoms, as was demonstrated for the completely nonmagnetic $t_{\text{nom}}=0.3$ nm sample in Fig. 3.

The two characteristic ranges of the Fe layer thickness, as observed in the temperature dependence of the magnetic properties, are also easily distinguished in the magnetic field

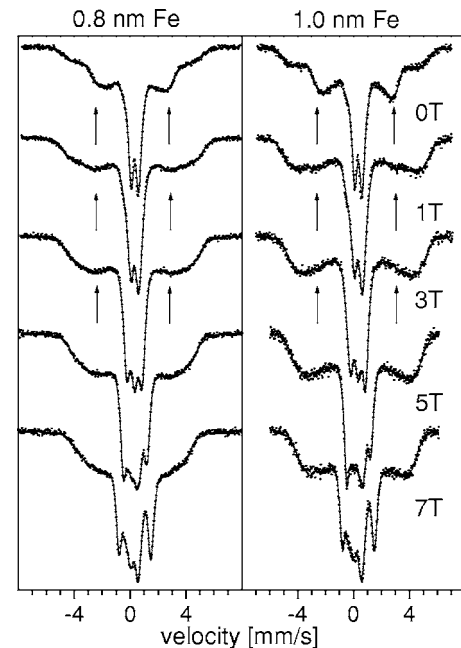


FIG. 11. Mössbauer spectra at 4.2 K in external magnetic fields B_{ext} applied perpendicularly to the sample plane of the $t_{\text{nom}}=0.8$ and 1.0 nm samples. The positions of the 2–5 lines belonging to $\langle B_h \rangle$ are marked by arrows for $B_{\text{ext}}=0$, 1, and 3 T, respectively.

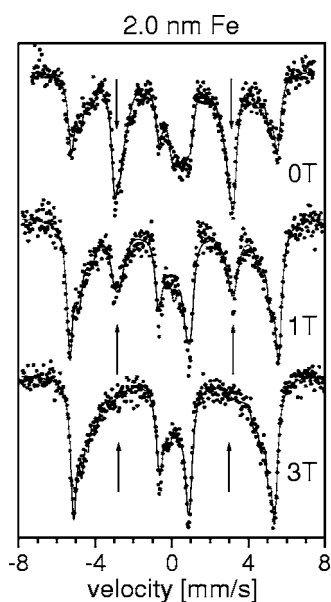


FIG. 12. Mössbauer spectra at 4.2 K in external magnetic fields B_{ext} applied perpendicularly to the sample plane of the $t_{\text{nom}}=2.0$ nm sample. The positions of the 2–5 lines belonging to $\langle B_h \rangle$ are marked by arrows.

dependence of the parameters. Samples consisting of two ML thick Fe platelets are practically not affected by the external magnetic field of 3 T, as shown in Fig. 10. In larger fields a decrease of the hyperfine field of the magnetic components (outer spectrum lines) is observed. As a result, however, the overlap with the broadening spectral contribution of the nonmagnetic Fe atoms strongly increases with increasing field and it prevents a reliable evaluation of the spectra. It is worth noting that Fe-Ag multilayers of similar nominal layer thickness and freezing temperature could be well aligned in a 3 T external field.⁴²

When applying $B_{\text{ext}}=3$ T field (which is well above 2.2 T, the demagnetizing field of bulk α -Fe in perpendicular geometry) the complete saturation (i.e., disappearance of the 2–5 lines) was observed only for the $t_{\text{nom}}=2.0$ nm sample, as shown in Fig. 12. When the hyperfine field measured in $B_{\text{ext}}=3$ T is increased by the applied field, its value is higher by about 2 T than it was in zero magnetic field: This difference is due to a demagnetizing field very close to the bulk value. In this sample, the magnetic moments are in the sample plane when no magnetic field is applied as is required by the shape anisotropy. Accordingly, the value of I_{2-5} deduced from the fit of the spectrum is 4. The same $I_{2-5}=4$ value was found in Ref. 9 for a comparable layer thickness. This is the magnetic behavior expected for bulk samples with magnetic anisotropy in the order of that in α -Fe.

A gradual transition is observed between the two different behaviors described above: The magnetic anisotropy continuously increases with decreasing Fe layer thickness. For

$t_{\text{nom}}=0.8$ and 1.0 nm the intensity of the 2–5 lines decreases considerably for $B_{\text{ext}}=1$ T, but full saturation is not achieved in 3 T, as can be seen in Fig. 11. The decrease of I_{2-5} is larger for the 1.0 nm than for the 0.8 nm Fe layer thickness sample. The possible role of a small superparamagnetic fraction [see Fig. 9(b)] was examined at 100 K for this intermediate thickness range, but the application of a 1 T external field did not influence f_p , whereas the intensities of the 2–5 lines of the spectrum significantly decreased.

V. CONCLUSION

Temperature and magnetic field dependences of the Fe hyperfine fields (i.e., magnetic moments) were studied by ^{57}Fe Mössbauer spectroscopy in ultrathin Fe/Al multilayers with constant Al (3 nm) and varying (between 0.3 and 2.0 nm) Fe layer thickness. Interface mixing was shown to result in the formation of a nonmagnetic alloy phase. The effective thickness of the magnetic Fe layers was calculated from the amount of intermixed Fe atoms, $t_D=0.3$ nm in equivalent thickness for all the samples. The observed change in the shape of the hyperfine field distributions and the related jump of the average parameters with increasing effective thickness is explained by the building up of the magnetic Fe layers and by the respective roles of the two and three or more ML thick Fe regions. A markedly different temperature and magnetic field dependence of the magnetic behavior was observed below and above $t_{\text{eff}}=0.5$ nm, where the formation of Fe regions consisting of three and more atomic planes starts. At and above this thickness T_C is well above room temperature; the Fe hyperfine fields show a Bloch-type $T^{3/2}$ law decrease with increasing temperature. In magnetic fields applied perpendicularly to the sample plane a rather large magnetic anisotropy, i.e., slow approach to magnetic saturation, is observed. In 3 T full collinearity of the magnetic moments is reached only in the thickest ($t_{\text{eff}}=1.7$ nm) sample. Below $t_{\text{eff}}=0.5$ nm, the formation of two ML thick magnetic platelets was deduced from the hyperfine field distribution. The magnetically split component of the spectra disappears well below room temperature. It is a kind of freezing at $T_f=15$ and 40 K for $t_{\text{nom}}=0.4$ and 0.7 nm, respectively. The hyperfine field increases linearly with decreasing temperature below T_f . The superparamagnetic nature of the transition was verified by the application of a 1 T magnetic field above the freezing temperature which resulted in the reappearance of the magnetic splitting. Our preliminary magnetization measurements are in qualitative agreement with the results discussed earlier.

ACKNOWLEDGMENTS

This work was supported by the Hungarian Research Fund under OTKA projects T 31854, T 46795, and T 48965.

*Electronic address: kaptas@szfki.hu

- ¹E.g., J. F. Bobo, L. Gabillet, and M. Bibes, *J. Phys.: Condens. Matter* **16**, S471 (2004); R. Skomski, *ibid.* **15**, R841 (2003); K. De'Bell, A. B. MacIsaac, and J. P. Whitehead, *Rev. Mod. Phys.* **72**, 225 (2000); R. Allenspach, *J. Magn. Magn. Mater.* **129**, 160 (1999); F. J. Himpsel, J. E. Ortega, G. J. Mankey, and R. F. Willis, *Adv. Phys.* **47**, 511 (1998); L. M. Falicov, D. T. Pierce, S. D. Bader, R. Gronsky, K. B. Hathaway, H. J. Hopster, D. N. Lambeth, S. S. P. Parkin, G. Prinz, M. Salamon, I. K. Schuller, and R. H. Victoria, *J. Mater. Res.* **5**, 1299 (1990).
- ²P. Grünberg, *Phys. Today* **54**, 31 (2001).
- ³A. Simopoulos, in *Mössbauer Spectroscopy in Materials Science*, edited by M. Miglierini and D. Petridis (Kluwer Academic, Dordrecht, 1999), p. 227.
- ⁴M. Przybylski, *Hyperfine Interact.* **113**, 135 (1998).
- ⁵D. E. Bürgler, C. M. Schmidt, D. M. Schaller, F. Meisinger, R. Hofer, and H.-J. Güntherodt, *Phys. Rev. B* **56**, 4149 (1997); S. Amirthapandian, B. K. Panigrahi, S. Rajagopalan, A. Gupta, K. G. M. Nair, A. K. Tyagi, and A. Narayanasamy, *ibid.* **69**, 165411 (2004).
- ⁶J. Balogh, L. F. Kiss, A. Halbritter, I. Kézsmárki, and G. Mihály, *Solid State Commun.* **122**, 59 (2002); J. Balogh, D. Kaptás, T. Kemény, L. F. Kiss, T. Pusztai, and I. Vincze, *Hyperfine Interact.* **141/142**, 13 (2002).
- ⁷T. M. Srinivasan, H. Claus, R. Viswanathan, P. A. Beck, and D. I. Bardos, in *Phase Stability in Metals and Alloys*, edited by Rudman, Stringer and Jaffe (McGraw-Hill, New York, 1967), p. 151; I. Vincze, *Phys. Status Solidi A* **7**, K43 (1971).
- ⁸M. B. Stearns, *Phys. Rev.* **147**, 439 (1966); G. P. Huffman, *J. Appl. Phys.* **42**, 1606 (1971); I. Vincze and I. A. Campbell, *J. Phys. F: Met. Phys.* **3**, 647 (1973); S. A. Makhlof, M. Shiga, and K. Sumiyama, *J. Phys. Soc. Jpn.* **60**, 3537 (1991); B. Fultz and Z. Q. Gao, *Nucl. Instrum. Methods Phys. Res. B* **76**, 115 (1993); D. Kaptás, E. Sváb, Z. Somogyvári, G. André, L. F. Kiss, J. Balogh, L. Bujdosó, T. Kemény, and I. Vincze, *Phys. Rev. B* **73**, 012401 (2006).
- ⁹M. Carbuicchio, G. Palombarini, M. Rateo, and G. Ruggiero, *Philos. Mag. B* **76**, 425 (1997).
- ¹⁰M. Carbuicchio, C. Grazzi, M. Rateo, G. Ruggiero, and G. Turilli, *Nanostruct. Mater.* **11**, 775 (1999).
- ¹¹M. Carbuicchio, M. Rateo, G. Ruggiero, M. Solzi, and G. Turilli, *J. Magn. Magn. Mater.* **196-197**, 33 (1999).
- ¹²M. Carbuicchio, C. Grazzi, M. Rateo, G. Ruggiero, M. Solzi, and G. Turilli, *J. Magn. Magn. Mater.* **215-216**, 563 (2000).
- ¹³I. Vincze, *Nucl. Instrum. Methods Phys. Res.* **199**, 247 (1982).
- ¹⁴T. Geilman, J. Chevallier, M. Fanciulli, G. Weyer, V. Nevolin, and A. Zenkevitch, *Appl. Surf. Sci.* **109/110**, 570 (1997).
- ¹⁵J. Noetzel, H. Geisler, A. Gorbunov, R. Gorbunov, R. Dietsch, H. Mai, A. Mensch, W. Möller, W. Pompe, H. Reuther, A. Tselev, E. Wieser, and H. Worch, *Mater. Sci. Forum* **287-288**, 455 (1998); J. Noetzel, K. Brand, H. Geisler, A. Gorbunov, A. Tselev, E. Wieser, and W. Möller, *Appl. Phys. A: Mater. Sci. Process.* **68**, 497 (1999).
- ¹⁶L. M. Prudencio, I. D. Nogueira, J. C. Waerenborgh, A. P. Goncalves, O. Conde, and R. C. da Silva, *Surf. Coat. Technol.* **158-159**, 339 (2002).
- ¹⁷L. M. Gratton, A. Miotello, C. Tosello, D. C. Kothari, G. Principi, and A. Tomasi, *Nucl. Instrum. Methods Phys. Res. B* **59/60**, 541 (1991); J. L. Alexandre, M. A. Z. Vasconcellos, R. Hübler, S. R. Teixeira, and I. J. R. Baumvol, *ibid.* **80/81**, 436 (1993).
- ¹⁸S. Nasu, P. H. Shingu, K. N. Ishihara, and F. E. Fujita, *Hyperfine Interact.* **55**, 1043 (1990); F. Cardellini, C. Contini, R. Gupta, G. Mazzone, A. Montone, A. Perin, and G. Principi, *J. Mater. Sci.* **33**, 2519 (1998); S. Enzo, R. Frattini, G. Mulas, and G. Principi, *ibid.* **39**, 6333 (2004).
- ¹⁹V. P. Godbole, S. M. Chaudhari, S. V. Ghaisas, S. M. Kanetkar, S. B. Ogale, and V. G. Bhide, *Phys. Rev. B* **31**, 5703 (1985).
- ²⁰J.-F. Bobo, P. Delcroix, J.-C. Ousset, M.-F. Ravet, and M. Piecuch, *J. Magn. Magn. Mater.* **93**, 452 (1991).
- ²¹A. R. Chowdhury and A. E. Freitag, *J. Appl. Phys.* **79**, 6303 (1996).
- ²²D. Meyer, K. Richter, P. Paufler, P. Gawlitza, and T. Holz, *J. Appl. Phys.* **87**, 7218 (2000).
- ²³E. Fonda and A. Traverse, *J. Magn. Magn. Mater.* **268**, 292 (2004).
- ²⁴J. Bogner, W. Steiner, M. Reissner, P. Mohn, P. Blaha, K. Schwarz, R. Krachler, H. Ispert, and B. Sepiol, *Phys. Rev. B* **58**, 14922 (1998).
- ²⁵S. Takahashi, X. G. Li, and A. Chiba, *J. Phys.: Condens. Matter* **8**, 11243 (1996); S. Takahashi, H. Onodera, X. G. Li, and S. Miura, *ibid.* **9**, 9235 (1997).
- ²⁶L. F. Kiss, D. Kaptás, J. Balogh, L. Bujdosó, T. Kemény, I. Vincze, and J. Gubicza, *Phys. Rev. B* **70**, 012408 (2004).
- ²⁷G. Athanassiadis, G. Le Caer, J. Foct, and L. Rimlinger, *Phys. Status Solidi A* **40**, 425 (1977); K. Szymanski, M. Biernacka, L. Dobrzynski, K. Perzynska, K. Recko, D. Satula, J. Waliszewski, and P. Zaleski, *J. Magn. Magn. Mater.* **210**, 150 (2000).
- ²⁸M. B. Stearns, *Phys. Rev.* **168**, 588 (1968).
- ²⁹I. Vincze and L. Cser, *Phys. Status Solidi B* **50**, 709 (1972).
- ³⁰D. L. Mills, *J. Magn. Magn. Mater.* **100**, 515 (1991).
- ³¹P. Bruno, *Phys. Rev. B* **43**, 6015 (1991).
- ³²U. Krey, *J. Magn. Magn. Mater.* **268**, 277 (2004).
- ³³U. Köbler and A. Hoser, *Physica B* **362**, 295 (2005).
- ³⁴E. Della-Torre, L. H. Bennett, and R. E. Watson, *Phys. Rev. Lett.* **94**, 147210 (2005).
- ³⁵W. Kipferl, M. Sperl, T. Hagler, R. Meier, and G. Bayreuther, *J. Appl. Phys.* **97**, 10B313 (2005).
- ³⁶Z. Wu, V. Suresh Babu, M. S. Seehra, and W. Abdul-Razzaq, *Phys. Rev. B* **45**, 2285 (1992).
- ³⁷S. Mørup, *J. Magn. Magn. Mater.* **37**, 39 (1983); S. Mørup and H. Topsoe, *Appl. Phys.* **11**, 63 (1976).
- ³⁸Z. Q. Qiu, S. H. Mayer, C. J. Gutierrez, H. Tang, and J. C. Walker, *Phys. Rev. Lett.* **63**, 1649 (1989).
- ³⁹F. Bodker, S. Mørup, and S. Linderorth, *Phys. Rev. Lett.* **72**, 282 (1994).
- ⁴⁰S. Mørup, in *Magnetic Properties of Fine Particles*, edited by J. L. Dormann and D. Fiorani (Elsevier, Amsterdam, 1992), p. 125.
- ⁴¹C. J. Gutierrez, Z. Q. Qiu, H. Tang, M. D. Wiczorek, S. H. Mayer, and J. C. Walker, *Phys. Rev. B* **44**, 2190 (1991).
- ⁴²M. Csontos, J. Balogh, D. Kaptás, L. F. Kiss, A. Kovács, and G. Mihály, *Phys. Rev. B* **73**, 184412 (2006).